Computational Materials Science 173 (2020) 109397

Contents lists available at ScienceDirect

Computational Materials Science

journal homepage: www.elsevier.com/locate/commatsci

Amorphous boron carbide from ab initio simulations

Tevhide Ayça Yıldız, Murat Durandurdu

Materials Science & Mechanical Engineering Program and Department of Materials Science & Nanotechnology Engineering, Abdullah Gül University, Kayseri 38080, Turkey

ARTICLE INFO

Keywords:
Amorphous
Boron carbide
Hardness

ABSTRACT

An amorphous boron carbide (a-B_4C) model is generated by means of ab-initio molecular dynamics calculations within a generalized gradient approximation and its structural, mechanical and electrical features are discussed in details. The mean coordination number of B and C atoms is estimated to be 5.29 and 4.17, respectively. The pentagonal pyramid-like motifs for B atoms, having sixfold coordination, are the main building units in a-B_4C and some of which involve with the development of B_{12} icosahedra. On the other hand, the fourfold-coordinated units are the leading configurations for C atoms. Surprisingly the formation of C-C bonds is found to be less favorable in the noncrystalline network, compared to the crystal. a-B_4C is a semiconducting material having an energy band gap considerably less than that of the crystal. A noticeably decrease in the mechanical properties of B_4C is observed by amorphization. Nonetheless a-B_4C is categorized as a hard material due to its high Vickers hardness of about 24 GPa.

1. Introduction

Strong covalent solids like diamond and cubic boron nitrite (BN) are superhard materials. Boron carbide (B_4C), the most stable B-C compounds [1], is known as the third hardest crystal after diamond and cubic BN. B_4C has been attracted considerable attentions in recent years because its high hardness, lightweight and refractory features as well as superlative thermo mechanical and electrical properties [2]. It can be fabricated easily, for example, by means of plasma enhanced chemical vapor deposition (PECVD) [3]. B_4C has various practical applications and can be used, for instance, as cutting tools, wear resistant gears, and ballistic armors [4,5]. It can also find some applications in devices as diodes and transistors [5]. Since it is a good neutron absorber, it can be used to control reactivity in nuclear reactors [6]. Another functional application area of B_4C is the treatment of cancer by using neutron capture therapy [7].

B_4C can form crystal (polycrystals or single crystal) and amorphous phases. The atomic structure of the B_4C crystal is rather unique and has been comprehensively discussed in the literature throughout long years [8–14]. At the beginning, it was believed that it consisted of just B_{12} icosahedrons and C-C-C linear chains [15,16]. In later years, however, the Raman and NMR spectra analyses revealed that B_4C did indeed have $B_{11}C$ icosahedrons with C-B-C intericosahedral chains [1,10]. Nonetheless, there have still been some uncertainties about how B and C atoms are arranged in the B_4C unit cell. In order to develop its scientific and technological investigations, a greater understanding of its local structure is indeed crucial.

Amorphous boron carbide (a-B_4C), of an interest material, can obtainable under diverse experimental techniques such as irradiations [17], shock compression [18], scratch test [19,20], electric field [21], depressurization from high pressure [22] and shear deformations [23,24]. Yet, its local structure is far more complicated than the crystal since it is a random icosahedral network. The earlier studies proposed that the B atoms in the amorphous configuration have two type motifs such as $B_{11}C$ icosahedrons and C-B-C chains associated with the icosahedrons [25,26], similar to the crystal. However, the C-B-C chains were not observed in deposited amorphous films [27,28]. Consequently, depending on experimental preparation protocols, different local structures might exist for a-B_4C. As revealed by experiments, the diverse local structure can lead to the distinct mechanical properties for a-B_4C, for example, its hardness was reported to be between 20.8 and 33.8 GPa depending on deposition temperature [28].

Two theoretical efforts can be found in the literature to model a-B_4C so far. Yet they proposed the different chemical environments such as the existing of B_{12} molecules, a dissimilar coordination distribution etc., for it. In the first study, the models having 120 and 135 atoms were generated by using a quite fast quench rate (840 K/ps) [6]. In the second computational study [2], the amorphous model consisting of 216 atoms (154B atoms and 62C atoms) was created using cooling rates of 41.25 K/ps and 165 K/ps in different temperature ranges. Consequently, different quenching rates and size of supercells used in these studies are probably the main factors to observe a distinct

E-mail address: murat.durandurdu@agu.edu.tr (M. Durandurdu).

https://doi.org/10.1016/j.commatsci.2019.109397
Received 12 August 2019; Received in revised form 5 November 2019; Accepted 6 November 2019
Available online 24 November 2019
0927-0256/

microstructure for a-B_4C.

The main objective of this study is to generate a slightly larger a-B_4C model (320 atoms) using a slow cooling rate (66 K/ps), to focus on its short-range order and its electrical and mechanical features and to compare them with available data in the literature.

2. Computational method

In the present study, the SIESTA package program [29] within a pseudopotential method [30] was carried out to perform molecular dynamics (MD) simulations. The double zeta (DZ) as atomic orbital basis set for valence electrons was preferred. The Becke gradient exchange functional [31] and Lee, Yang, and Parr correlation functional [32] were chosen to calculate the exchange correlation energy. The grid mesh cutoff was applied as 120 Ry and the Brillouin zone integration was restricted to the Γ-point. The MD calculations were executed within the constant number of atom (N), pressure (P) and temperature (T). T and P were controlled by the velocity scaling and the Parrinelo-Rahman [33] approaches, separately. The MD time step was chosen to be 1.0 fs. Our initial configuration was a randomly distributed structure with 320 atoms (256B atoms and 64C atoms.) Firstly, the initial configuration was exposed to a temperature of 3200 K for 40 ps. Secondly; the temperature applied was decreased step by step from 3200 K to 300 K with a cooling rate of 66 K/ps. Finally, the structure was relaxed using a conjugate gradient technique. The crystalline form, a supercell having 120 atoms, was constructed based on $B_{11}C$and C-B-C chains as suggested in Ref. 1. In the present work, the density of amorphous and crystalline phases of B_4C is estimated to be 2.2493 g/cm^3 and 2.4471 g/cm^3, respectively, which are slightly less than 2.47 g/cm^3 (amorphous) and 2.52 g/cm^3 (crystal) reported in experiment obtained by using helium pycnometry [2]. It should be noted that in both studies, amorphization leads to a decrease in the density of B_4C, which is however contradict to Ref. 24 in which it was proposed that shear-induced or quenched amorphous phases have a larger density than the crystal.

3. Results

3.1. Local structure

The partial pair distribution functions (PPDFs) investigation is one of the convenient approaches to distinguish the microstructure of materials. Hence, firstly, we study PPDFs of the amorphous and crystalline forms of B_4C and illustrate them in Fig. 1. Since the bonding natures (B-B, B-C and C-C) play a crucial role in determining the structure and properties of a-B_4C, the first peak of all pairs is carefully examined. The first peak of the B-B, B-C and C-C correlations of a-B_4C (B_4C crystal) is located at nearly 1.77 Å (1.77 Å), 1.58 Å (1.62 Å) and 1.49 Å (1.56 Å), respectively. So one can see a slight shortening in the B-C and C-C bond lengths by amorphization. Our values logically agree with the computational results of 1.75 Å (B-B), 1.57 Å (B-C) and 1.54 Å (C-C) reported for a-B_4C [2]. The strength of the first C-C peak is relatively smaller than that of the first B-B and B-C peaks because of the presence of the limited number of C-C bonds in the amorphous arrangement, meaning that the formation of C-C bonds is not very favorable in the amorphous network (see below for the chemical environment analysis). The visible second and third peaks of B-B correlation are a result of pentagonal pyramids/B_{12} icosahedral molecules formed in the noncrystalline structure.

The total and partial coordination numbers (CNs) and chemical distribution analyses are very necessary to expose the microstructure of the materials in details. Therefore, we secondly estimate them for each species using the first minimum of PPDFs (~2.22 Å for B-B, ~2.19 Å for B-C and ~2.24 Å for C-C correlations). The coordination distribution of the atoms is shown in Fig. 2. In the a-B_4C model, B atoms have a coordination distribution ranging from 2 to 7. Amongst them, six-fold coordination is the most dominated one with a fraction of nearly 48.0%

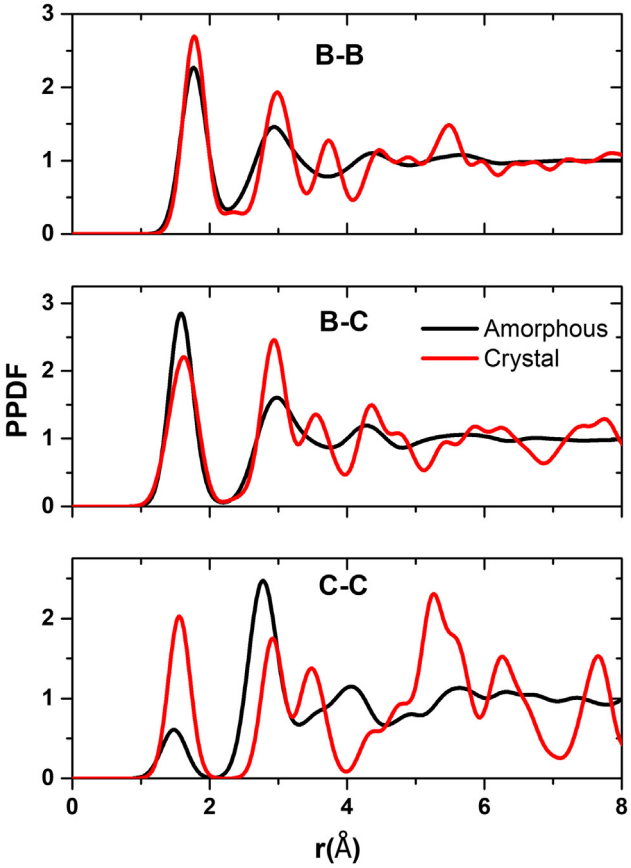

Fig. 1. Partial pair distribution functions of a-B_4C and B_4C crystal.

(see also Table 1), which is slightly higher than the value of 42.90% reported in Ref 2. Our amorphous arrangement has three-fold (10%) and four-fold (10.54%) coordinated B atoms, which are less than 15% and 18.80% recounted in Ref 2. However, our disordered configuration demonstrates about 4% more five-fold and seven-fold coordinated motifs relative to the a-B_4C model of Ref. 2 (see Table 1). These coordination distributions result in an average CN of B atoms to be 5.29, which is comparable with 5.66 in the crystal. For C atoms, the most prevalent cluster is the four-fold coordinated unit (68.75%) and its fraction is again comparable with 61.3% stated in the earlier study [2]. The second and third dominant motifs are the five-fold (21.87%) and three-fold (7.80%) coordination, slightly different than 29% and 4.9% reported in Ref 2. The mean CN of C atoms is 4.17, parallel to 4.66 in the crystal. All these observations reveal the striking similarities between our model and previously proposed amorphous network [2] and the crystal.

For a-B_4C, the chemical environments of B and C atoms demonstrated in Table 2 can provide more knowledge about the system at the microscopic level. As seen from Table 2, the most prevalent clusters for B atoms are B-B_5C_1 (23.83%) and B-B_6 (20.31%) type motifs. On the other hand, in the crystalline B_4C structure, B atoms have four kind motifs: B-B_5C_1 (50.00%), B-B_6 (25%), B-B_4C_2 (16.67%) and B-C_2 (8.33%). Here B-C_2 unit represents the intericosahedral linear C-B-C chain and as seen in Table 2, it does not exist in the noncrystalline network. Nonetheless one can see that nearly 50% of B atoms in the a-B_4C model form clusters (B-B_5C_1, B-B_6 etc.), similar to those of the crystal, suggestion partial local similarities between these two forms of B_4C. The first three common configurations for C atoms are C-B_4 (57.81%), C-B_5 (20.31%) and C-B_3C_1 (10.94%) kind units. Likewise, the crystalline B_4C contains C-B_4 (33.33%), C- B_3C_1 (33.33%) and C-B_5C_1 (33.33%) type structures. The formation of more C-B_4 and less C-B_3C_1 kind units and the lack of C-B_5C_1 type clusters in the amorphous model

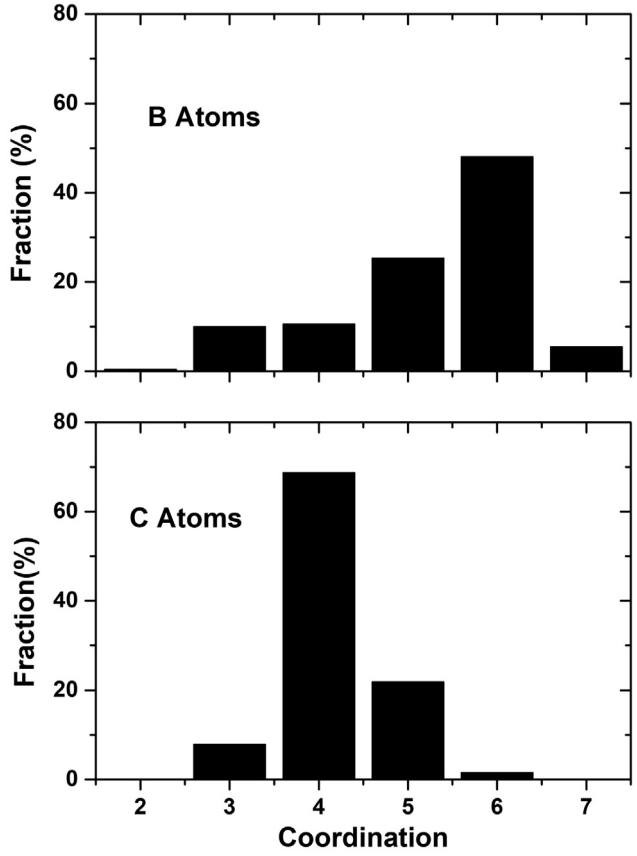

Fig. 2. Coordination distribution of the amorphous model.

Table 1
Coordination distribution of B and C atoms in the a-B_4C.

1st Neighbors	2	3	4	5	6	7	References
B (%)	0.39	10	10.54	25.30	48.04	5.46	This study
	0	15	18.80	21.40	42.90	1.9	[2]
C (%)	0	7.80	68.75	21.87	1.50	0	This study
	0	4.90	61.30	29.00	4.80	0	[2]

Table 2
Chemical identities around B and C atoms for a-B_4C.

a-B_4C			
B		C	
B_5C_1	23.83%	B_4	57.81%
B_6	20.31%	B_5	20.31%
B_4C_1	9.77%	B_3C_1	10.94%
B_5	7.03%	B_3	3.12%
B_3C_2	6.64%	B_2C_1	3.12%
B_1C_2	5.86%	B_4C_1	1.56%
B_4C_2	4.30%	B_1C_2	1.56%
B_3C_1	3.12%	B_6	1.56%
B_2C_2	3.12%		
B_7	2.73%		
B_4	2.34%		
B_2C_1	2.34%		
C_3	1.95%		
B_2C_3	1.95%		
B_1C_3	1.56%		
B_6C_1	1.56%		
B_3C_3	0.78%		
B_3	0.39%		
B_1C_1	0.39%		

relative to the crystal can be interpreted as the tendency of C atoms to form more C-B bonds than C-C bonds in the amorphous model and their trend to form more tetrahedral configurations.

With aid of the Voronoi polyhedral approach [34], one can distinguish the type of clusters shaped around B and C atoms and thus have valuable information on the structure at the atomistic level. In this method, the indices $< n_3, n_4, n_5, n_6 \ldots >$ are used to identify polyhedrons, where n_i and Σn_i stand for the number of i-edge faces of a polyhedron and its CN, respectively. The principal structural unit of B and B-rich crystalline/amorphous materials is known as B_{12} molecules, which comprises of pentagonal pyramids [35]. In the crystalline B_4C phase, the most favorable polyhedron is characterized by $< 2, 2, 2, 0 >$ index (92%), which represents the pentagonal pyramid. In other respects, we find eight distinct polyhedra for B atoms in the disordered structure. The two leading ones are denoted by the $< 2, 2, 2, 0 >$ (47%) and $< 2, 3, 0, 0 >$ (24%). Here the second one can be classified as defective pentagonal pyramid-like structures. Subsequently one can see that about 70% of B atoms have a tendency to form complete or incomplete pentagonal pyramid-like patterns in the amorphous network. On the other hand, we determine three diverse polyhedra for C atoms in a-B_4C. The most foremost ones are labeled as $< 4, 0, 0, 0 >$ (68%) and $< 2, 3, 0, 0 >$ (21%). In addition, we find $< 2, 2, 2, 0 >$ (0.01%) type cluster, a part of $B_{12}C$ molecules. In the ordered form, on the other hand, there are just two types of polyhedrons for C atoms and they are characterized by the $< 4, 0, 0, 0 >$ (66%) and $< 2, 2, 2, 0 >$ (33%) indices. All these findings specify partial similarities in the local structure of amorphous and crystalline forms of B_4C. The earlier study [2] suggests the formation of B_{12}, $B_{11}C$ and $B_{10}C_2$ molecules for a-B_4C. Yet our model has just B_{12} and $B_{12}C$ molecules. The lack of the other clusters in our network might be associated with the size of simulation boxes or different cooling rates used in present and earlier studies.

To identify the structure features of a-B_4C in details, we further analyze the bond angle distribution functions (BADFs) and compare them with those of the crystalline structure. The B-B-B, B-C-B and C-B-C angle distributions for the crystal and a- B_4C are shown in Fig. 3. The B-B-B angles produce two main peaks. The first peak is located at 59° while the second peak is positioned at nearly 107°, similar to the crystalline B_4C phase. These two sharp peaks are related to the intraicosahedral bonds of the pentagonal pyramids. The third sharp peak at around 122° in the crystal are associated with the intericosahedral bonds and weakly presented in the amorphous model due to the randomly distributed icosahedrons (or pentagonal pyramids). The B-C-B angles of the crystalline structure have three sharp peaks at around 62°, 99° and 113°, which are again related to the intraicosahedral and intericosahedral bonds. These B-C-B angles show a broad distribution in our model but the peaks around 62°, 99° and 113° angles are roughly produced in our model. The C-B-C distribution in the noncrystalline network ranges from 90° and 180° and has a foremost peak at nearly 120°, which slightly deviates from 123° presented in the crystal. The C-B-C at 180° is not captured in the amorphous network. The occurrence of these peaks suggests the existence of C-B-C bonds in the amorphous configuration but the intericosahedral linear C-B-C chain does not exist since B-C_2 motif does not form in the model (see Table 2), which is also confirmed by visualizing the model given in Fig. 4.

3.2. Electronic properties

Boron-rich materials such as the crystalline and amorphous boron carbides are of great interest for numerous technological applications, particularly, in the semiconductor devices. For that reason, revealing the electronic behaviors of the ordered and disordered B_4C structures is significant in this study. Firstly, the electronic properties of a-B_4C and the crystal are investigated via the total electron density of states (TDOS). Secondly, in order to get more detailed contribution about their electronic features, their partial electron density of states (PDOS) is calculated. Fig. 5 illustrates them. The band gap energy for the B_4C

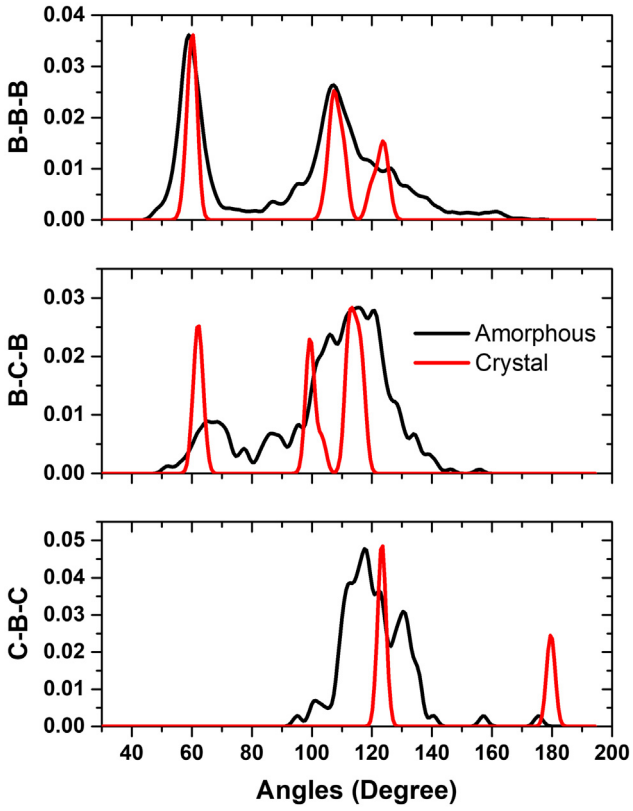

Fig. 3. Bond angle distribution functions of a-B_4C and B_4C crystal.

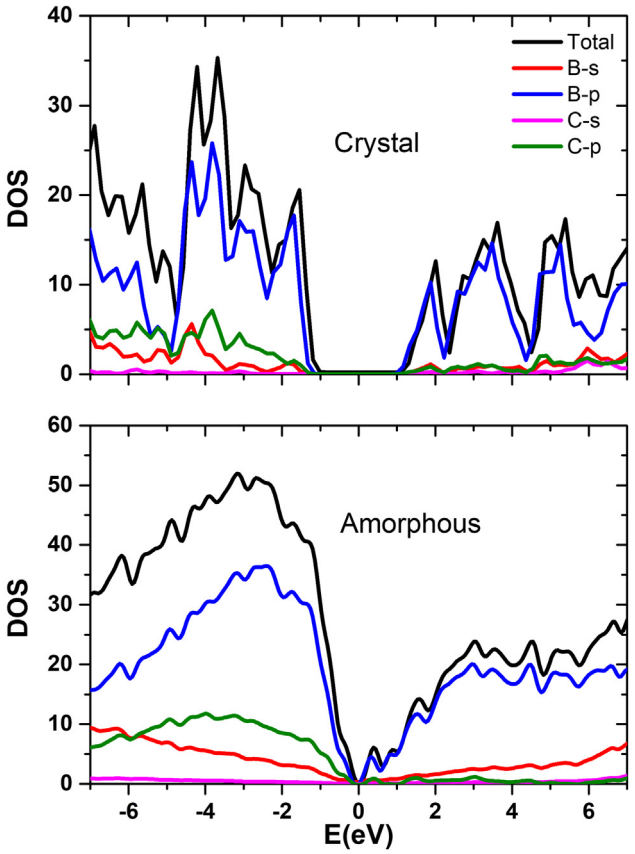

Fig. 5. Total electron density of states (TDOS) and partial density of state (PDOS).

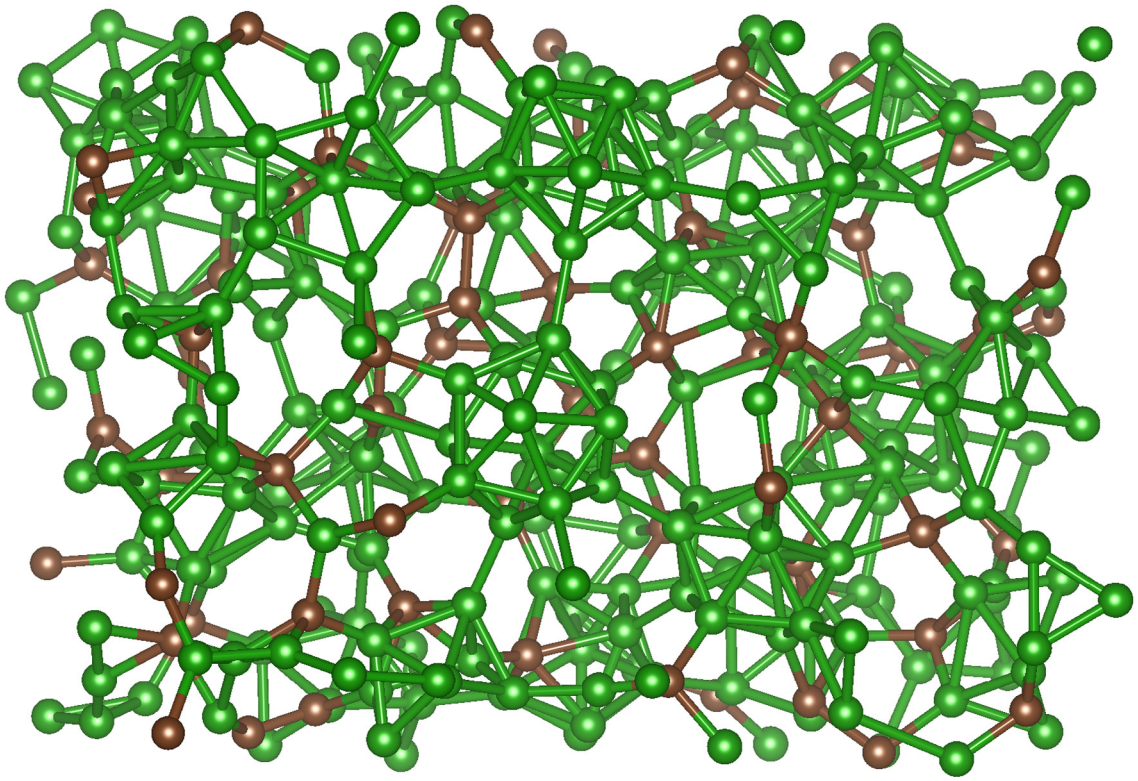

Fig. 4. Ball-stick representation of a-B_4C.

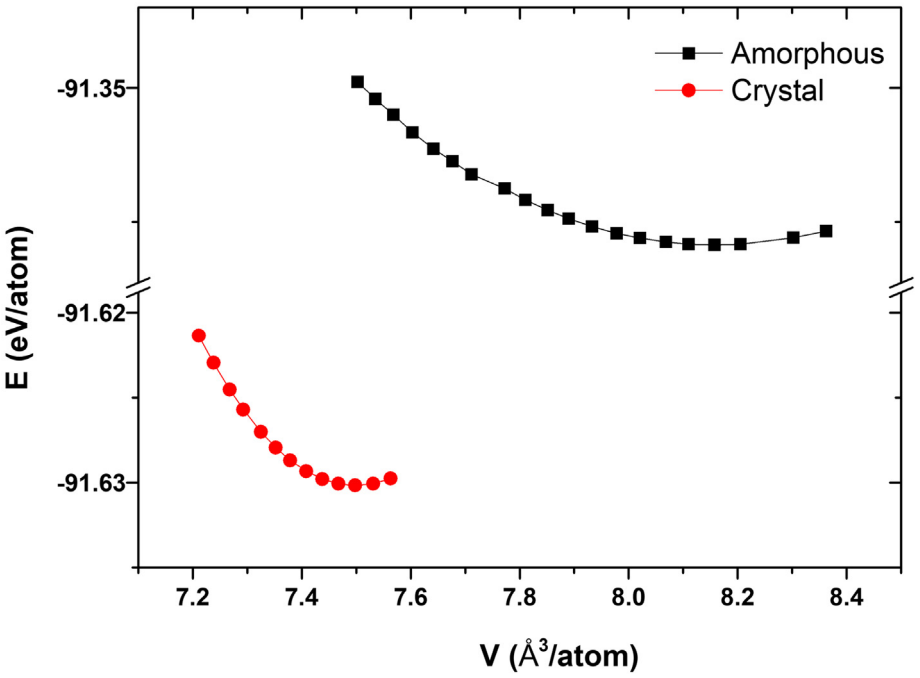

Fig. 6. Energy volume relation of a-B_4C and B_4C crystal.

crystal is nearly 2.9 eV, parallel to the previous DFT-GGA (LDA) band gap of 2.6–3.0 eV [6,11,36–38]. It should be noted here that GGA calculations lead to smaller energy band gaps relative to experiments due to the self-interaction error in DFT-GGA computations. Such a limitation can be eliminated by using DFT-GGA + U, DFT-GWA or DFT-hybrid exchange functionals (HEFs). Indeed, using a HEF, the band gap energy of the crystal was estimated to be 3.84 eV [39]. In other respect, the energy band gap of a-B_4C is found as 0.15 eV. Thus, a drastic band gap closure is observed by amorphization but not metallization as suggested in Ref.6. According to the PDOS analysis, B-p states are more prevailing for both valence and conduction bands of the amorphous and crystalline phases. Additionally, B-s and C-p states also have some contributions to the valence band for both structures. However, C-s states have minor effect on the bands for the noncrystalline network, similar to the crystal.

3.3. Mechanical properties

As a beginning, the relation between energy (E) and volume (V) for the crystalline and amorphous states is determined via a variable cell optimization technique. We estimate their bulk modulus (K), and equilibrium volume (V_0) and energy (E_0) by fitting the E-V values given in Fig. 6 to the third-order Birch-Murnaghan equations of states,

$$E(V)E_0 + \frac{9V_0K}{16}\left\{\left[\left(\frac{V_0}{V}\right)^{\frac{2}{3}} - 1\right]^3 K' + \left[\left(\frac{V_0}{V}\right)^{\frac{2}{3}} - 1\right]^2\left[6 - 4\left(\frac{V_0}{V}\right)^{\frac{2}{3}}\right]\right\}.$$

As deduced from the Fig. 5, the crystal has lower energy than the amorphous state. The relative energy difference between them is predicted to be around 0.25 eV/atom. The equilibrium volume of the crystal is 7.49 Å^3/atom whereas that of the amorphous structure is about 8.16 Å^3/atom. Thus one can notice about 9% volume expansion by amorphization.

In Table 3, we list the mechanical properties of a-B_4C and the crystal along with the data available in the literature. The K value of a-B_4C is estimated to be about 162.61 GPa while that of the crystalline form is nearly 245 GPa, in good agreement with the earlier predictions of 248–274 GPa [1,40,41,44,48]. Consequently, amorphization leads to a noticeably decrease in the bulk modulus which is related to the disorder nature (coordination defects, fraction of chemical defects etc.) of the amorphous model.

We apply a uniaxial stress along the principle axes of the supercells and optimize the atomic coordinates and their volume to predict the Poisson's ratio (ν) defined by

$$\nu_{ij} = -\frac{\Delta L_i/L_i}{\Delta L_j/L_j}$$

here L_s are the magnitude of supercells' vectors and i and j denote x, y and z directions (in the formula j represents the compressed direction and i signifies the lateral direction). Poisson's ratio is predicted from the slope of the best fitting straight line and six different values between 0.16 and 0.21 are obtained for the noncrystalline network. The calculated average Poisson's ratio for the amorphous and crystalline forms of B_4C is about 0.18 and 0.17 respectively, which is quite in agreement with the results of the earlier studies as presented in Table 3 [40–42].

Knowing K and ν is enough to compute the Young's modulus (elastic modulus) (E) using the following relation

$$E = 3K(1 - 2\nu).$$

E is estimated to be 312 GPa for a-B_4C, which is reasonably in the range of experimental values of 255–351 GPa reported for a-B_4C at different temperatures [28]. For the ordered form, it is 470 GPa that again coincides with 402–441 GPa [40–42,43].

The shear modulus (μ) is another important mechanical property of a material and can be obtained by using the next equation:

$$\mu = \frac{E}{2(1+\nu)}$$

The shear modulus computed for a-B_4C is about 132 GPa. For the crystalline form, the modulus is estimated to be around 200 GPa, which is quite akin to the available results of 188–200 GPa [40–42,43,48] in the literature.

In the last step, the Vickers hardness (H_v) is calculated using three different empirical equations. The first formula, called as Teter's equation, is given by the following formula [45]

$$H_v = 0.151\mu$$

The second equation, known as Chen's equation [46], is given by

Table 3
Bulk modulus (K), Young's modulus (E), shear modulus (μ), hardness (H) and Poisson ratio (ν) in the crystalline and amorphous structures. References 19, 28, 40, and 41 are the experimental data.

	K(GPa)	E(GPa)	μ (GPa)	K/μ	ν	H (GPa)	References
Crystal	245	470	200	1.22	0.17	~32 (Chen)	This study
						~30 (Teter)	This study
						~31 (Tian)	This study
	248, 274						[1]
						~40, 41	[19]
		402				~42	[28]
	235	462	197		0.17		[40]
	247	472	200		0.18		[41]
		448			0.21		[42]
		441	188				[43]
	239					~45	[44]
	238		199				[48]
				1.20		~32	[49]
Amorphous	162.61	312.22	132.29	1.23	0.18	~24 (Chen)	This study
						~20 (Teter)	This study
						~23 (Tian)	This study
		255–351				~21–34	[28]

the next relation,

$$H_v = 2\left(\frac{\mu}{n^2}\right)^{0.585} - 3(\text{GPa})$$

where n is equal to K/μ and known as Pugh's ratio.

The Chen's equation appears to have some limitation and was revised by Tian [47] as follows

$$H_v = 0.92\left(\frac{1}{n}\right)^{1.137}(\mu)^{0.708}.$$

By using these three useful equations, the Vickers hardness of the disordered model is projected to be between 20 and 24 GPa, reasonably in the range of previous results of 21–34 GPa reported for a-B_4C [25]. On the other hand, for the crystal, we calculate its Vickers's hardness to be about 30–32 GPa, which are slightly smaller than previous experimental data of 40–42 GPa [19,28,49].

Pugh's ratio can be used to reveal the brittle or ductile behavior of a material. The critical value for n is equal to 1.75. If n is higher (lower) than 1.75, then the material is ductile (brittle). n is 1.23 for a-B_4C and 1.22 for the crystal, showing their brittle character. These values are in quite good agreement with earlier result of 1.20 [49] as seen in Table 3.

4. Conclusions

We have carried out a comprehensive investigation on the local structure, electronic properties, and mechanical features of a-B_4C via quantum mechanical MD simulations. Our structural parameters are found to be close to those of the previous investigations. The local structure of the amorphous model is partially similar to that of the crystal. The C–C bonds are found to be less favorable in the non-crystalline network. The mean coordination number of B and C atoms for a-B_4C is 5.29 and 4.17, correspondingly. The amorphous configuration shows an energy band gap of 0.15 eV, strikingly smaller than 2.9 eV estimated for the crystal. Softening of the mechanical properties is observed by amorphization. Nonetheless, a-B_4C can be classified as a hard material due to its high Vickers hardness.

CRediT authorship contribution statement

Tevhide Ayça Yıldız: Data curation, Formal analysis, Investigation, Visualization, Writing - original draft. **Murat Durandurdu:** Conceptualization, Funding acquisition, Methodology, Project administration, Resources, Software, Supervision, Validation, Writing - review & editing.

Acknowledgements

This research was supported by the Scientific and Technological Research Council of Turkey (TÜBİTAK) under grant number 117M372. The simulations were performed using the TÜBİTAK ULAKBİM-TRUBA resources.

Data availability

The raw/processed data required to reproduce these findings cannot be shared at this time as the data also forms part of an ongoing study.

References

[1] R. Lazzari, N. Vast, J.M. Besson, S. Baroni, A. Dal Corso, Phys. Rev. Lett. 83 (1999) 3230.
[2] C. Pallier, J.M. Leyssale, L.A. Truflandier, A.T. Bui, P. Weisbecker, C. Gervais, G. Chollon, Chem. Mater. 25 (2013) 2618–2629.
[3] S. Lee, J. Mazurowski, G. Ramseyer, P.A. Dowben, J. Appl. Phys. 72 (1992) 4925–4933.
[4] A.W. Weimer, Thermochemistry and kinetics. In Carbide, nitride and boride materials synthesis and processing, Springer, Dordrecht, 1997, pp. 79–113.
[5] F. Thevenot, J. Eur. Ceram. Soc. 6 (1990) 205–225.
[6] V.I. Ivashchenko, V.I. Shevchenko, P.E.A. Turchi, Phys. Rev. B 80 (2009) 235208.
[7] M.W. Mortensen, P.G. Sørensen, O. Björkdahl, M.R. Jensen, H.J.G. Gundersen, T. Bjørnholm, App. Radiat. Isot. 64 (2006) 315–324.
[8] A. Lipp, "Boron Carbide: Production, Properties, Applications" (in Ger.), Tech. Rundsch. 58 (1966) 1–47.
[9] J.L. Hoard, R.E. Hughes, Elemental Boron and Compounds of High Boron Content: Structure, Properties,and Polymorphism. In The Chemistry of Boron and Its Compounds; Muetterties, E. L. Ed.; Wiley, New York, 1967.
[10] Nathalie Vast, J. Sjakste, E. Betranhandy, J. Phys.: Conf. Seri. 176 (2009) 012002–012003.
[11] K. Shirai, J. Superhard Mater. 32 (2010) 205–225.
[12] K. Shirai, J. Superhard Mater. 32 (2010) 336–345.
[13] A.K. Suri, C. Subramanian, J.K. Sonber, T.C. Murthy, Int. Mater. Rev. 55 (2010) 4–40.
[14] H. Werheit, V. Filipov, U. Kuhlmann, U. Schwarz, M. Armbrüster, A. Leithe-Jasper, A.M.M. Korsukova, Sci. Technol. Adv. Mat. 11 (2010) 023001.
[15] H.K. Clark, J.L. Hoard, J. Am. Chem. Soc. 65 (1943) 2115–2119.
[16] G.S. Zhdanov, N.G. Sevast'yanov, ZhFH 52 (1943) 326–335.
[17] D. Simeone, C. Mallet, P. Dubuisson, G. Baldinozzi, C. Gervais, J. Maquet, J. Nucl. Mater. 277 (2000) 1–10.
[18] M.W. Chen, J.W. McCauley, K.J. Hemker, Science 299 (2003) 1563–1566.
[19] V. Domnich, Y. Gogotsi, M. Trenary, T. Tanaka, App. Phys. Lett. 81 (2002) 3783–3785.
[20] D. Ge, V. Domnich, T. Juliano, E.A. Stach, Y. Gogotsi, Acta Mater. 52 (2004) 3921–3927.
[21] G. Fanchini, V. Gupta, A.B. Mann, M. Chhowalla, J. Am. Ceram. Soc. 91 (2008) 2666–2669.
[22] X.Q. Yan, Z. Tang, L. Zhang, J.J. Guo, C.Q. Jin, Y. Zhang, M.W. Chen, Phys. Rev. Lett. 102 (2009) 075505.
[23] Q. An, W.A. Goddard III, T. Cheng, Phys. Rev. Lett. 113 (2014) 095501.
[24] Q. An, W.A. Goddard III, Phys. Rev. Lett. 115 (2015) 105501.

[25] K. Shirai, S. Emura, S.I. Gonda, Y. Kumashiro, J. Appl. Phys. 78 (1995) 3392–3400.
[26] M.J. Zhou, S.F. Wong, C.W. Ong, Q. Li, Thin Solid Films 516 (2007) 336–339.
[27] L.G. Jacobsohn, M. Nastasi, Surf. Coat. Technol. 200 (2005) 1472–1475.
[28] V. Kulikovsky, V. Vorlicek, P. Bohac, R. Ctvrtlik, M. Stranyanek, A. Dejneka, L. Jastrabik, Diamond Relat. Mater. 18 (2009) 27–33.
[29] J.M. Soler, E. Artacho, J.D. Gale, A. García, J. Junquera, P. Ordejón, D. Sánchez-Portal, J. Phys.: Condens. Matter. 14 (2002) 2745.
[30] N. Troullier, J.L. Martins, Phys. Rev. B 43 (1991) 1993.
[31] A.D. Becke, Phys. Rev. A 38 (1988) 3098.
[32] C. Lee, W. Yang, R.G. Parr, Phys. Rev. B 37 (1988) (1988) 785.
[33] M. Parrinello, A. Rahman, J. Appl. Phys. 52 (1981) (1981) 7182–7190.
[34] N.N. Medvedev, J. Comput. Phys. 67 (1986) 223–229.
[35] A.Ö. Cetin, M. Durandurdu, J. Am. Ceram. Soc. 101 (2018) (2018) 1929–1939.
[36] A. Ektarawong, S.I. Simak, B. Alling, Phys. Rev. Mater. 2 (2018) 104603.
[37] D.M. Bylander, L. Kleinman, S. Lee, Phy. Rev. B 42 (1990) 1394.
[38] A. Ektarawong, S.I. Simak, L. Hultman, J. Birch, B. Alling, Phys. Rev. B 90 (2014) 024204.
[39] H. Wang, Q. An, Am. J. Phys. Chem. (2019) 12505–12513.
[40] M.H. Manghnani, Y. Wang, F. Li, P. Zinin, W. Rafaniello, Sci. Technol. High Pressure 2 (2000) 25–30.
[41] J.H. Gieske, T.L. Aselage, D. Emin, AIP Conference Proceedings. 231 (1991) 65–76.
[42] S.R. Murthy, J. Mater. Sci. Lett. 4 (1985) 603–605.
[43] K.A. Schwetz, W. Grellner, J. Less Common Met. 82 (1981) 37–47.
[44] S. Aydin, M. Simsek, Phys. Status Solidi B 246 (2009) 62–70.
[45] D.M. Teter, Mrs Bull. 23 (1998) 22–27.
[46] X.Q. Chen, H. Niu, D. Li, Y. Li, Intermetallics 19 (2011) 1275–1281.
[47] Y. Tian, B. Xu, Z. Zhao, Int. J. Refract. Met. Hard Mater. 33 (2012) 93–106.
[48] Y. Shen, G. Li, Q. An, Scr. Mater. 162 (2019) 306–310.
[49] Q. An, W.A. Goddard III, J. Phys. Chem. Lett. 5 (2014) 4169–4174.